THE JOURNAL OF PHYSICAL CHEMISTRY B

Article

pubs.acs.org/JPCB

Protein Influence on Charge-Asymmetry of the Primary Donor in Photosynthetic Bacterial Reaction Centers Containing a Heterodimer: Effects on Photophysical Properties and Electron Transfer

Michelle A. Harris,[†] Craig A. Luehr,[‡] Kaitlyn M. Faries,[†] Marc Wander,[‡] Lucas Kressel,[‡] Dewey Holten,[†] Deborah K. Hanson,[‡] Philip D. Laible,[‡] and Christine Kirmaier*[,†]

[†]Department of Chemistry, Washington University, St. Louis, Missouri 63130, United States

[‡]Biosciences Division, Argonne National Laboratory, Argonne, Illinois 60439, United States

Supporting Information

ABSTRACT: The substantial electronic distinctions between bacteriochlorophyll (BChl) and its Mg-free analogue bacteriopheophytin (BPh) are exploited in two sets of *Rhodobacter capsulatus* reaction center (RC) mutants that contain a heterodimeric BChl−BPh primary electron donor (D). The BPh component of the M-heterodimer (Mhd) or L-heterodimer (Lhd) obtains from substituting a Leu for His M200 or for His L173, respectively. Lhd-β and Mhd-β RCs serve as the initial templates in the two mutant sets, where β denotes that the L-side BPh acceptor (H_L) has been replaced by a BChl (due to substituting His for Leu M212). Three variants each of Lhd-β and Mhd-β mutants were constructed: (1) a swap (denoted YF) of the native Phe (L181) and Tyr (M208) residues, which flank D and the nearby M- and L-side monomeric BChl cofactors, respectively, giving Tyr (L181) and Phe (M208); (2) addition of a hydrogen bond (denoted L131LH) to the ring V keto group of the L-macrocycle of D, via replacing the native Leu at L131 with His; (3) the combination of 1 and 2. A low yield of electron transfer (ET) to the M-side BPh (H_M) is observed in all four Lhd-containing RCs. Comparison with the yield of ET to β on the L-side shows that electron density on the L-macrocycle of D* favors ET to the M-side cofactors and vice versa. Increasing or decreasing the electronic asymmetry of D* via the YF, L131LH mutations or the combination results in consistent trends in the characteristics of the long-wavelength ground state absorption band of D, the rate constant of internal conversion of D* to the ground state, and the rate constants for ET to both the L- and M-side cofactors. A surprising correlation is that an increase in the charge asymmetry in D* not only increases the D* internal-conversion rate constant, but also the rate constants for ET to both the L- and M-side cofactors, spanning time scales of tens of picoseconds to several nanoseconds. The YF swap has a previously unrecognized effect on the electronic asymmetry of D*, resulting in increased charge asymmetry for the Mhd and decreased charge asymmetry for the Lhd. This result indicates that the native Tyr (M208) and Phe (L181) in the wild-type RC promote an electron distribution in P* that is the *reverse* of that favorable for ET to the photoactive L-branch. This conclusion reinforces the view that the native configuration of these residues promotes ET to the L branch primarily by poising the free energies of the charge-separated states. Overall, this work addresses the extent to which electronic couplings complement energetics in underpinning the directionality of ET in the bacterial RC.

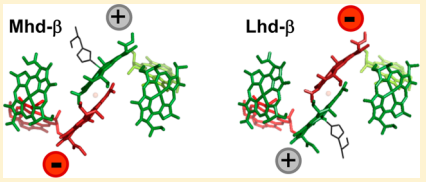

INTRODUCTION

The bacterial photosynthetic reaction center (RC) is comprised of three polypeptide subunits designated L, M, and H and symmetry-related branches of bacteriochlorophyll (BChl or B), bacteriopheophytin (BPh or H) and quinone (Q) cofactors. RCs contain a dimeric "special pair" of BChls denoted P that is the lowest energy trap for light absorbed by the chromophores on the antenna proteins in situ or, for isolated RCs, by the RC chromophores themselves.[1−5] A near-unity yield of charge separation is effected from the singlet excited state P* and maintained through successive electron transfer (ET) steps to the B_L, H_L and Q_A cofactors culminating in formation of $P^+Q_A^-$ in less than a nanosecond (Figure 1A). Owing to its estimated placement below P* in free energy by 50−100 meV and above $P^+H_L^-$ by 150−200 meV, $P^+B_L^-$ is a strategically poised intermediate that facilitates overall ∼3 ps ET from P* to H_L, whereas $P^+B_M^-$, which is (presumed) higher in free energy than P*, can support ET to H_M only via a superexchange mechanism (Figure 2A). [In a superexchange mechanism P* → $P^+H_M^-$ utilizes the orbitals of B_M as an electron conduit, but $P^+B_M^-$ is not formed as a discrete intermediate.] The M-side chromophores, in pseudo-C_2 symmetry to the L-side chromophores, have been shown to provide much slower and much lower yielding P* → $P^+H_M^-$ → $P^+Q_B^-$ ET steps, with ET from P* to H_M having an ∼100 ps time constant in wild-type RCs.[6−8] The primary strategy to alter the relative rates and yields of L- versus M-side ET has been to change amino acids near B_L or B_M with the intent of raising the free energy of $P^+B_L^-$ or lowering that of $P^+B_M^-$.[9] The tenet that one is rationally altering the free energies of these states and thus

Received: January 31, 2013
Revised: March 12, 2013

   dx.doi.org/10.1021/jp401138h | J. Phys. Chem. B XXXX, XXX, XXX−XXX

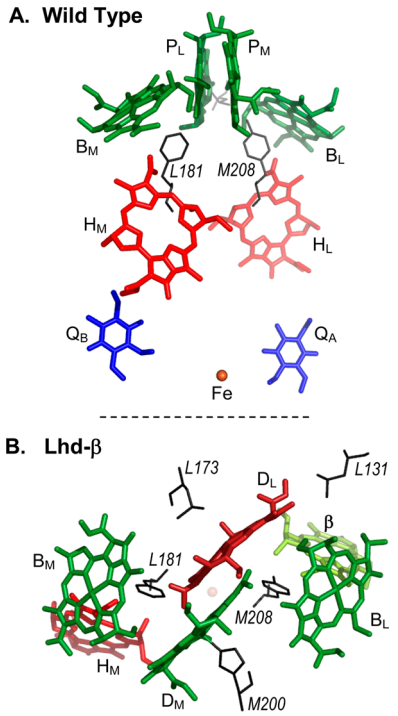

Figure 1. Reaction center cofactors and sites of mutation based on the wild-type *Rb. sphaeroides* crystal structure (2j8c in the Protein Data Bank[1]) with BChl (green), BPh (red), quinone (blue), and Fe atom (orange). Lighter-shaded pigments indicate dimensionality and that the cofactor is "behind" or "underneath" other cofactors. (A) Wild-type RCs. In this view, L131 is rendered between and behind the two rings of P and is not labeled. (B) Model for Lhd-β RCs, looking down the C_2 symmetry axis from the heterodimer toward the Fe atom. Residue M200 is the native His ligand to the dimer's BChl moiety D_M. L173, C_2 symmetry-related to M200 and a His in wild-type, is changed to Leu resulting in BPh in place of BChl for the D_L macrocycle. The β pigment replaces H_L. The two quinones are not shown in this view.

altering the rates, yields and/or mechanism of initial charge separation to the L- and M-cofactors, is drawn by inference from consistent observation of ET to H_M at the expense of ET to H_L in a variety of mutants.

In addition to energetics, the directionality of charge separation to the L-side versus the M-side depends on differences in electronic interactions between P and the cofactors on the two branches. The combination of these factors determines the rate of an ET reaction as given by $k_{ET} = V^2 \cdot FC$. The Franck–Condon (FC) factor relates the reaction's overall free energy change and reorganization energy and consequently is sensitive to the relative free energies of the charge-separated states. In turn, these free energies are affected by amino acid changes that directly or indirectly alter the redox properties of a cofactor. The electronic term V^2 takes into account the orbital overlap between P and the acceptor chromophores (i.e., distances) and the electron-density distributions in P* and the charge-separated states. Clearly there is no way to rationally manipulate the distances between the cofactors. Theoretical studies have examined the inherent biasing of electronic asymmetry in the excited state of P*, the special contributions of a dimeric ET donor, and the relative electronic couplings between P* and B_L versus between P* and B_M.[10−36] Electron-density distributions in P* and P^+ are asymmetric due to local and global differences in the dielectric environment experienced by P_L and P_M. For example, P_L has a hydrogen bond (from His L168) to the acetyl group of ring I, whereas P_M does not. P_L and P_M denote the two BChl macrocycles of P and the associated polypeptide that provides the His ligand: His L173 for P_L and His M200 for P_M. Electron nuclear double resonance (ENDOR) and electron spin resonance (ESR) experiments have shown that the hole in P^+ visits both halves of the dimer but is not shared equally and can be altered by mutations such as adding/deleting hydrogen bonds.[37−40]

For P*, electronic asymmetry derives from the relative contributions (mixing) of the locally excited configurations

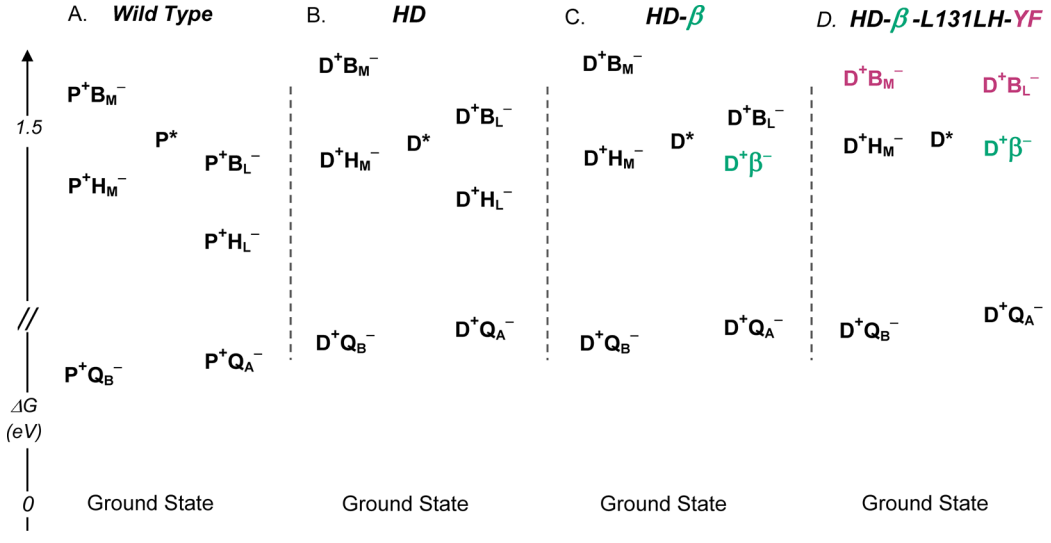

Figure 2. Schematic free-energy diagrams for the RCs indicated; HD refers to heterodimer. P* is roughly 1.4 eV above the ground state and $P^+Q_A^-$ and $P^+Q_B^-$ are ~0.6 eV above the ground state in wild-type. The free energies of the states ≥1.0 eV are roughly to scale and show the qualitative relative changes proposed for the mutations. Key differences between the panels are as follows. Compared to wild-type in part A, analogous states in the other panels are at higher free energy because D is harder to oxidize than P. In parts C and D, the changes due to β are in teal with $D^+\beta^-$ higher in free energy than $D^+H_L^-$. In part D, the changes due to YF are in maroon with $D^+B_M^-$ and $D^+B_L^-$ placed at comparable free energy. The L131H mutation in part D raises the free energies of all the charge-separated states.

dx.doi.org/10.1021/jp401138h | J. Phys. Chem. B XXXX, XXX, XXX–XXX

$P_L^*P_M$ and $P_LP_M^*$ (linear combinations of which are the exciton configurations) and the charge-transfer (CT) configurations $P_L^+P_M^-$ and $P_L^-P_M^+$ (linear combinations of which are the charge-resonance configurations).[41,42] The energies of the CT configurations are particularly sensitive to the dielectric of the environment. The degree of net CT character of P* (derived from the difference in the contributions of $P_L^+P_M^-$ and $P_L^-P_M^+$) has been invoked in describing the ground state absorption band of P,[12,17,18,23−26] hole-burning and Stark effect spectra,[11,43−54] properties of the dimer triplet state,[55−58] and the directionality and mechanism of initial charge separation.[13−19,31,36,59] Both calculations and experiments have suggested that the protein asymmetry imparts a small net $P_L^+P_M^-$ CT character to P* in the wild-type RC.[13,16,18,20,21,25,27,36,60]

In heterodimer RCs, the primary electron donor (D) consists of a BChl-BPh pair, the BPh replacing a BChl upon loss of the His ligand to that BChl's central Mg^{2+} ion.[61−66] The L-heterodimer (Lhd), depicted in Figure 1B, derives from substituting Leu for His at L173. Changing the symmetry-related His M200 to Leu gives the M-heterodimer (Mhd). A number of studies have indicated that D* in heterodimer RCs has more CT character than P* in wild type.[25,41,49,50,54,60,63,67−71] Heterodimer RCs are uniquely suited to the purpose of examining how electron-density distribution in the donor excited state affects relative branching of ET to the L- and M-cofactors.[69] This obtains from the combination of D* having significant charge asymmetry and ET to both the L- and M-sides occurring by superexchange (*vida infra*).

Relative to wild-type (Figure 2A), in the heterodimers (whether Lhd or Mhd) the equivalent charge-separated states are at higher free energy owing to the 150−200 mV higher (more positive) oxidation potential of D compared to P.[66,68,71,72] Thus it is plausible that $D^+B_L^-$ is higher in free energy than D* (Figure 2B), and previous work on heterodimer mutants demonstrating much slower ET to H_L than in wild-type is consistent with this placement. Under this model, initial charge separation in heterodimer RCs would occur from D* to both the L- and M-side via a superexchange mechanism. Near equalization of the free energies of the initial L- and M-side charge-separated products is afforded in heterodimer RCs containing a BChl (denoted β) in place of H_L. This chromophore change results from mutation of a Leu near H_L (residue M212) to His.[73,74] For heterodimer-β RCs (Figure 2C), $D^+\beta^-$ is placed higher in free energy compared to $D^+H_L^-$ (in Figure 2B); this shift follows because BChl is 100−150 mV harder to reduce than BPh in vitro.[75,76] Thus in heterodimer-β RCs, the free energies of the two ET reactions D* → $D^+\beta^-$ (L-side) and D* →$D^+H_M^-$ (M-side) can be presumed nearly equal.

Clearly, however, D* in Lhd RCs and D* in Mhd RCs have opposite electronic biasing because of the substantial, perhaps dominant, contributions of opposite CT configurations: $D_L^-D_M^+$ in Lhd and $D_L^+D_M^-$ in Mhd. This situation, coupled with the well-matched free energies of $D^+\beta^-$ and $D^+H_M^-$ (Figure 2C) and the equivalency of ET by a superexchange mechanism to both the L-side and M-side allowed us in previous work to use Lhd-β and Mhd-β to address the relative contributions of the electronic factor (V), distinct from the Franck−Condon factor (FC), for ET to the L- versus the M-side in these RCs. Extrapolating to wild-type, we concluded that the electronic factor contributes at most ∼35% to unidirectional L-side ET in wild-type RCs, with the majority effect deriving from energetic considerations, i.e., differences in the free energies of the charge-separated states, reorganization energies and one- versus two-step mechanisms on the two sides of wild-type RCs.[69] Additionally, from comparison of the yields of ET to H_M in Lhd-β (∼6%) and Mhd-β (∼1.5%), we determined for the first time that higher electron density on the L-macrocycle of D* favors ET to the M-side and conversely that higher electron density on the M-macrocycle of D* favors ET to the L-side.[69] Previous theoretical studies on heterodimer[30] and wild-type[13,14,16,18,25,29,30] RCs had indicated that the M macrocycle of the primary electron donor has a stronger electronic interaction with B_L than B_M, and vice versa for the L macrocycle of the dimer. Previous experiments had shown that P* in wild-type RCs has net $P_L^+P_M^-$ CT character.[60] Together these three findings lead naturally to the suggestion that a design criterion to bias electron transfer to the L-side in native RCs would be to endow P* with some net $P_L^+P_M^-$ CT character in order to weight electron density toward the M macrocycle.

To test and advance these ideas further, we have expanded our investigation of heterodimer RCs with two new sets of *Rb. capsulatus* Lhd and Mhd mutants. The Lhd set consists of Lhd-β and three new variants denoted Lhd-β-YF, Lhd-β-L131LH, and Lhd-β-L131LH-YF. The Mhd set consists of Mhd-β and the three parallel additions of YF, L131LH, and the combination of both. YF was chosen because we expect it to better balance the energetics, while L131LH was chosen for its primary effects on the electronic asymmetry of D*.

YF denotes a pair swap, where the native Phe at L181 is changed to Tyr and the C_2-symmetry-related native Tyr at M208 is changed to Phe (Figure 1). Both calculations[20,21,27,77] and experiments[8,78−88] have indicated that the native Y at M208 lowers the free energy of $P^+B_L^-$, while F at L181 provides no similar stabilization of $P^+B_M^-$. This difference is thought to be a main agent of fast two-step ET to H_L via B_L in wild-type (Figure 2A). Calculations and redox measurements have indicated that there is little *net* effect on the P oxidation potential in wild-type upon the swap of FY to YF at the L181-M208 pair.[77,84] The goal of the YF swap here is to equalize better and selectively the (free) energies of $D^+B_M^-$ and $D^+B_L^-$, lowering the former and raising the latter (compare panels D and C in Figure 2). Such a change would balance off differences in the energy denominators for the electronic mixing (V) terms in the superexchange formulations for D* → $D^+\beta^-$ versus D* → $D^+H_M^-$. We are not aware of previous work that addresses whether or how the nature of the residues at L181 and M208 affects the electron-density distribution in P* (wild-type) or D* (heterodimers). Results obtained here provide new insight on this point.

The second mutation we have used is denoted L131LH, where a His replaces the native Leu at L131. This His is in favorable position to form a hydrogen bond to the ring V keto group of the L-macrocycle of the dimer (Figure 1B) and experiments have confirmed such for both P and D.[39,40,68,71,89−96] This hydrogen bond increases the oxidation potential of both P and D by 80−100 mV,[68,89,90,92,96] uniformly raising the free energies of all the charge-separated states yet again (Figure 2D). However, the targeted effect of L131LH is to affect the charge asymmetry of D*. L131LH is expected to have an electron withdrawing effect on the dimer's L macrocycle, increasing or "pulling" electron density onto that macrocycle from the M macrocycle. Stark effect measurements

dx.doi.org/10.1021/jp401138h | J. Phys. Chem. B XXXX, XXX, XXX−XXX

Table 1. Effects of L131LH and YF on Photophysical Properties of Lhd and Mhd Mutants

mutant	D^* lifetime (ps)	ϕ_G (% yield ground state)	ϕ_L (% yield $P^+\beta^-$)	ϕ_M (% yield $D^+H_M^-$)	$(k_G)^{-1}$ (ps)[a]	$(k_L)^{-1}$ (ps)[a]	$(k_M)^{-1}$ (ps)[a]	k_L/k_M
Lhd-β	30 ± 2	95	3	2	32	1000	1500	1.5
Lhd-β-YF	41 ± 4	95	4	1	43	1025	4100	4.0
Lhd-β-L131LH	15 ± 2	92	4	4	16	375	375	1.0
Lhd-β-L131LH-YF	21 ± 2	93	5	2	23	420	1050	2.5
Mhd-β	26 ± 4	94	5−6	<1	28	435−520	>2600	>5
Mhd-β-YF	25 ± 4	93	6−7	<1	27	355−415	>2500	>6
Mhd-β-L131LH	53 ± 5	97	2−3	<1	55	1765−2650	>5300	>2
Mhd-β-L131LH-YF	50 ± 5	96	3−4	<1	52	1250−1650	>5000	>3

[a]Time constants for the three D^* decay processes: internal conversion to the ground state $[(k_G)^{-1}]$, ET to β on the L-side $[(k_L)^{-1}]$, and ET to H_M on the M-side $[(k_M)^{-1}]$.

on *Rhodobacter (Rb.) sphaeroides* L131LH RCs have shown this to be the case.[60] The L131LH mutation should induce opposite effects on D* in the Lhd and Mhd mutants in terms of the magnitude of electronic asymmetry. L131LH should cooperatively increase the electronic asymmetry of D* in the L-heterodimer where D_L is a BPh but reduce the electronic asymmetry inherent to D* in the M-heterodimer where D_M is a BPh. On the basis of our previous work, a prediction for Lhd-β-L131LH is that ET to H_M would be increased compared to Lhd-β. Such a result is obtained here. The present study extends our previous work[69] on heterodimer RCs and addresses the contribution of electronic coupling, distinct from considerations of energetics, to the directionality of initial ET in the bacterial photosynthetic RC.

EXPERIMENTAL SECTION

The RC mutants of *Rb. capsulatus* studied here are listed in column 1 of Table 1. The Lhd-β and Mhd-β mutants were reported previously.[69] The other six mutants that additionally incorporate L131LH (Leu at L131 changed to His), YF (Phe at L181 changed to Tyr and Tyr at M208 changed to Phe), or both are new. Strains were constructed following standard methods previously described.[8,80,97] Briefly, oligonucleotide-directed mutagenesis was performed according to directions from a kit (QuikChange; Stratagene), and the presence of the correct mutations was verified with didoxy sequencing (ACGT, Inc.). All of the RCs carry a heptahistidine tag on the C-terminus of the M subunit and were purified by immobilized metal affinity chromatography with some steps benefitting from semiautomated procedures.[80,98] RC integrity and purity was assessed spectroscopically by comparing the pigment absorption bands in the visible and near-infrared (NIR) and/or protein absorbance at 280 nm. In the present work, Deriphat 160C was used to purify RCs owing to prior experience that this milder detergent often achieves better yields of difficult-to-isolate RCs. While sufficient protein was obtained for the studies, we found (as in the past) that the RC yields from the Lhd mutants were poorer than for the Mhd mutants. All experiments were performed with RCs in 10 mM Tris pH 7.8 buffer containing 0.1% Deriphat 160C.

Ultrafast time-resolved transient absorption (TA) measurements utilized a Ti-sapphire-based laser system running at 10 Hz and providing ∼130 fs excitation pulses (full-width-at-half-maximum 10−13 nm) at 850 or 590 nm and white-light probe flashes. Samples of ∼2 mL volume were held at ∼285 K in an ice-cooled reservoir and flowed through a 2 mm path length optical cell. Further details of the laser and spectrometer instrumentation and data analysis procedures were as previously described.[8]

RESULTS

The ground state absorption spectra of Lhd-β, Lhd-β-L131LH, Lhd-β-YF, and Lhd-β-L131LH-YF and those for the analogous set of Mhd-containing RCs are shown in Figures 3A and 3B,

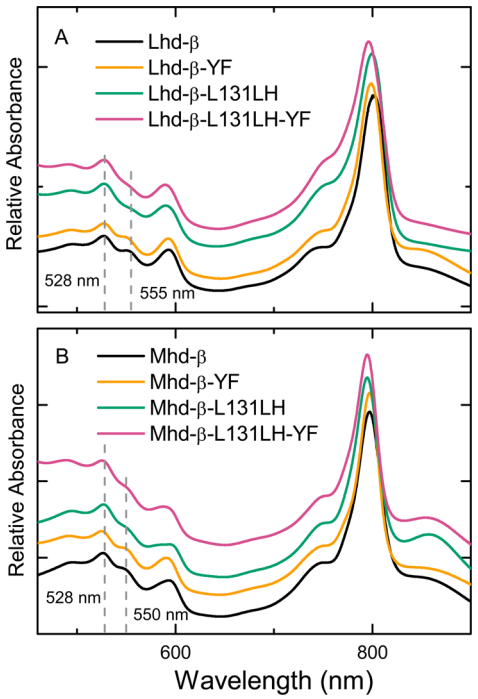

Figure 3. Room-temperature ground state absorption spectra of RCs from the Lhd (A) and Mhd (B) mutant sets. The spectra have been normalized at 800 nm and offset for clarity. The dotted lines are positional guides at the wavelengths indicated.

respectively. The 865-nm long-wavelength absorption band of the native BChl−BChl dimer P (Figure S1) is replaced with much weaker NIR absorption of the BChl-BPh heterodimer D. While noting that the RC's carotenoid contributes to the broad absorption profile from ∼450−580 nm, a peak or shoulder between 550 and 555 nm is consistently revealed in all the spectra in Figure 3. This feature has been assigned as a monomer-like Q_X absorption band of the BPh component of D. An analogous monomer-like Q_X absorption band of the BChl component of D is expected but not clearly resolved at 295 K in the 580−610 nm absorption envelope shared by the

dx.doi.org/10.1021/jp401138h | J. Phys. Chem. B XXXX, XXX, XXX−XXX

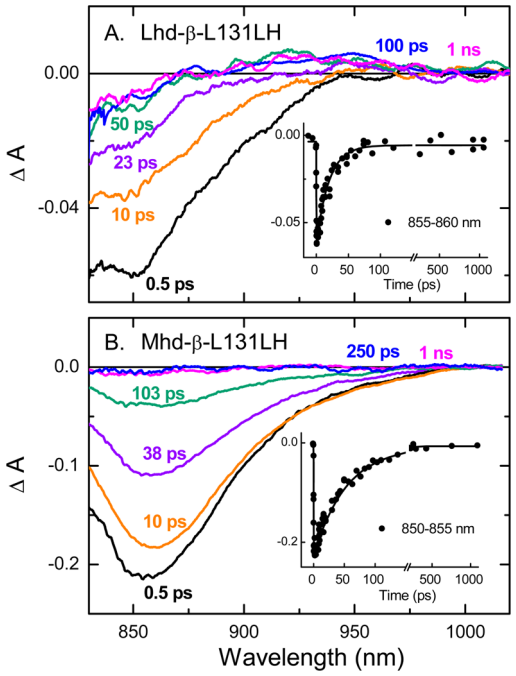

Figure 4. Main: transient absorption spectra acquired at the times indicated following a 130-fs 590-nm excitation flash for Lhd-β-L131LH (A) and Mhd-β-L131LH (B). The insets show the time course of the TA data averaged over the 5-nm intervals indicated (circles) and a fit to the instrument function plus one exponential and a constant (solid line).

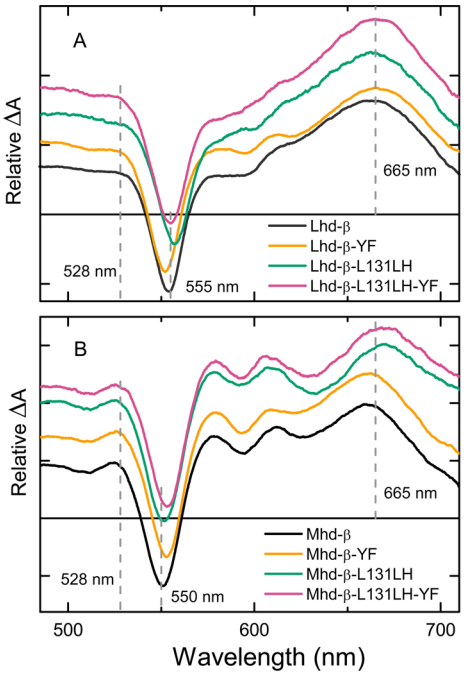

Figure 5. Transient absorption spectra of D* in the sets of Lhd (A) and Mhd (B) mutants. The spectra were acquired 0.5 ps after an ~130-fs excitation flash at 850 nm and have been normalized to the same bleaching at ~555 nm (A) or ~550 nm (B) and offset for clarity. The dotted lines are positional guides at the wavelengths indicated.

four BChls in these β-containing heterodimer RCs. The Q_X band of H_M is resolved in the spectra in Figure 3 at ~528 nm.

Figure 4A shows NIR TA spectra for Lhd-β-L131LH (main panel) and kinetic data for the decay of D-bleaching and a fit to the instrument response plus one exponential plus a constant (inset). Analogous spectra and kinetic data and fit for Mhd-β-L131LH are given in Figure 4B. (Spectra for the other six mutants are given in Figures S2, S3 and S4.) Bleaching of the long wavelength absorption of D upon formation of D* is evident in the 0.5 ps spectra. As seen in Figure 4 (and Figures S2–S4 for the other six mutants), <10% of the D bleaching remains following D* decay, indicating that >90% of D* has returned to the ground state via internal conversion. The magnitude of the small D bleaching that remains following D* decay relative to the initial magnitude of D bleaching is a measure of the total yield of charge-separated products formed from D*. Table 1 columns 2 and 3 give the D* lifetimes and percent yield of D* → ground state, respectively, for the eight mutants as determined from the NIR D-bleaching data.

TA spectra of D* in the two sets of Lhd and Mhd mutants acquired in the 500–700 nm region, encompassing the Q_X bands of the chromophores, are shown in Figures 5A and 5B, respectively. (For comparison, the wild-type P* spectrum is shown in Figure S5.) The main features of these spectra are bleaching near 550 nm and a broad absorption to the red with a peak between 660 and 670 nm. The broad absorption band, much like that of the broad ~665 nm H_L anion (observed in the spectrum of $P^+H_L^-$ in wild-type RCs), is a defining characteristic that originally led to the suggestion that the heterodimer excited state D* has significant contribution of the $[D_{(BPh)}^-][D_{(BChl)}^+]$ CT configuration.[41,67] The D* spectra of the four Mhd mutants have a small feature near 590 nm that could be bleaching of a BChl absorption. For the four Lhd mutants, such a feature is less resolved in the D* spectra. For each mutant, the yields of charge separation to β on the L-side and to H_M on the M-side were predicated on comparison of the mutant's initial D* spectrum acquired at 0.5 ps to the spectrum acquired at a time equal to six D* lifetimes (i.e., at a time corresponding to six 1/e lifetimes of D* decay). TA spectra of the charge-separated states formed following D* decay (the "six-lifetimes" spectra) for the Lhd mutants are shown in Figure 6. All four spectra reveal bleaching of the H_M ground state absorption band at 528 nm, which is a marker for ET to H_M.

To determine the yield of ET to H_M, we followed the procedure used in our previous work.[6-8,69] Specifically, for each mutant, the 528 nm bleaching profile in the "six-lifetimes"

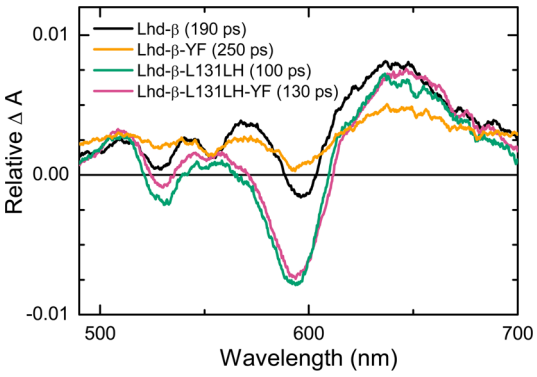

Figure 6. Transient absorption spectra of the charge-separated states formed following D* decay in the Lhd mutants. The spectra were acquired at the times indicated following excitation at 850 nm, in each case corresponding to roughly six multiples of the D* lifetime in that mutant. The spectra have been offset slightly from one another for clarity of display.

dx.doi.org/10.1021/jp401138h | J. Phys. Chem. B XXXX, XXX, XXX–XXX

Table 2. Photophysical Properties of Heterodimer-Containing Mutants in Different Detergents

mutant	D* lifetime (ps)	ϕ_G (% yield ground state)	ϕ_L (% yield L-side ET)	ϕ_M (% yield M-side ET)	$(k_G)^{-1}$ (ps)	$(k_L)^{-1}$ (ps)	$(k_M)^{-1}$ (ps)	k_L/k_M
Lhd (LDAO)[a,b]	25 ± 5	70	≤30	n.d.	36	≥83	n.d.	n.d.
Lhd (Deriphat)[a]	23 ± 2	73	≤27	n.d.	32	≥88	n.d.	n.d.
Lhd-β (LDAO)[b]	40 ± 8	85	9	6	47	444	670	1.5
Lhd-β (Deriphat)[c]	30 ± 2	95	3	2	32	1000	1500	1.5
Mhd (LDAO)[a,b]	14 ± 4	75	≤25	n.d.	19	≥56	n.d.	n.d.
Mhd (Deriphat)[a]	22 ± 5	70	≤30	n.d.	31	≥73	n.d.	n.d.
Mhd-β (LDAO)[b]	15 ± 5	93	5.5	1.5	16	273	1000	3.7
Mhd-β (Deriphat)[c]	26 ± 4	94	5−6	<1	28	433−520	>2600	>5

[a]Since the Lhd and Mhd mutants contain the native H_L, it is not possible to determine the yield of ET to H_M in these mutants; hence this yield and the associated time constants are not determined (n.d.) for these. [b]Reported in ref 47. [c]Also reported in Table 1.

spectrum was fit to a Gaussian and the value compared to (divided by) the value of the Gaussian fit of the initial ∼550 nm bleaching (in the 0.5 ps spectrum of that mutant). This ratio gives the yield of ET to H_M under the assumption that the oscillator strengths of the ∼550 nm absorption band of D and the ∼528 nm absorption band of H_M are equal. [Here we are interested in comparing the trends among the four Lhd mutants and similarly among the four Mhd mutants. Even if the absolute yields are off by a certain factor, the trends and comparisons among the four mutants in a set are valid under the less stringent criteria that the absorption properties at ∼550 nm are constant within the set.]

Using Lhd-β as an example, the ratio of the integrated 528 nm bleaching in the "six-lifetimes" spectrum to the integrated 550-nm bleaching of D* at 0.5 ps is 0.02. This value is reported in Table 1 column 5 as a 2% yield of ET to H_M. Such a low yield of ET to H_M is independently established above by the D bleaching data in the NIR, wherein D* is found to decay 95% to the ground state, leaving only 5% total charge-separated products (Table 1 column 3). This agreement supports (virtually establishes) the validity of approximately equal oscillator strengths of H_M at 528 nm and the BPh moiety of D at ∼550 nm for the Lhd mutants. Subtraction of the 2% yield of M-side ET to H_M from the 5% total yield of charge separation gives the 3% L-side ET to β reported in column 4 of Table 1 for Lhd-β. Similar analysis of each mutant was carried out. The results are given in columns 4 and 5 of Table 1. Using the observed yields (ϕ_i) of the three products of D* decay, and a simple trifurcated model for D* decay, rate constants for D* return to the ground state (k_G), for ET from D* to β on the L side (k_L) and for ET from D* to H_M (k_M) were calculated from the formula $k_i = \phi_i/\tau$, where τ is the D* lifetime. Columns 6, 7, and 8 in Table 1 give the time constants so calculated (where the time constant is equal to $1/k_i$).

Table 2 compares our new results for Lhd, Lhd-β, Mhd, and Mhd-β RCs isolated using Deriphat with our previous results for the same mutants isolated using LDAO.[69] For the simple Lhd and Mhd RCs (which retain the native H_L cofactor), it is not possible to cleanly determine a yield of ET to H_M from the bleaching at 528 nm because of the overlapping bleaching at 542 nm due to ET to H_L. Thus, for the simple Lhd and Mhd RCs, a yield of ET to H_M is not reported in Table 2, and the yield of ET to the L-side (to H_L) is an upper limit, simply the arithmetic result of subtracting from 100 the observed yield of D* decay to the ground state given in column 3. Similarly, k_M and k_L/k_M for these two mutants (last two columns of Table 2) are not determined.

DISCUSSION

Evidence that L131LH Provides a Hydrogen Bond to the L-Macrycocle of D. The TA spectra of D* in the four Lhd mutants provide evidence that the His introduced at L131 forms a hydrogen bond to the ring V keto group of the L-moiety of D (Figure 1B). As described above (and below), the Q_X bands of the two macrocycles of the heterodimer D may largely retain monomer-like molecular origin. If so, the bleaching near 555 nm in the Lhd mutants and near 550 nm in the Mhd mutants both largely monitor absorption of the BPh moiety of D. For Lhd-β, this Q_X absorption band (reflected in the bleaching position in Figure 5A) is at 554 nm, while for Lhd-β-L131LH it is at 558 nm. Comparison of the Q_X bleachings for Lhd-β-YF (552 nm) and Lhd-β-L131LH-YF (555 nm) reveals a similar red-shift due to L131LH. These red-shifts are consistent with previous studies of the effects of hydrogen bonds in wild-type and mutant RCs. For example, the Q_X band of H_L, which has a native hydrogen bond to its ring V keto group (via Glu L104), is at 542 nm. Upon removal of this hydrogen bond, the H_L absorbance shifts to the blue.[99] The 528-nm Q_X band of the non-hydrogen bonded native H_M is red-shifted upon addition of a hydrogen bond to its ring V keto group (via replacing Leu at M131L with Asp).[83,94,100] In some regard, the four M-heterodimer mutants provide a control for this effect. Here, the position of bleaching of the BPh-like Q_X band of D is not noticeably shifted by L131LH (Figure 5B). For the Mhd mutants, the BPh reporting at ∼550 nm is (presumably) the M-moiety of D, which is not the macrocycle that residue L131 neighbors (Figure 1B). Thus no shift of the ∼550 nm band is expected when L131LH is introduced.

Near-Infrared Absorption of D. Compared to the BChl dimer P, the BChl−BPh heterodimer D has a much reduced NIR absorption band, in many cases manifesting only as a weak broad tail at longer wavelengths than the 800-nm absorption band of the monomeric BChls (B_L and B_M) as shown in Figure 3. A number of previous studies have addressed the changed nature of the NIR heterodimer absorption band and origin in increased CT character of D* compared to P*.[25,41,49,50,54,60,63,67−71] Net CT character (electronic asymmetry) of P* and D* has been quantified by Stark effect measurements in a systematic study of a series of *Rb. sphaeroides* wild-type and Mhd mutants, including both L131LH and Mhd-L131LH.[60] That work demonstrated that as the charge distribution in D* becomes more asymmetric the long wavelength absorption band of D becomes less distinct (broader and weaker).

The ground state absorption spectra in Figure 3 show qualitative trends that are consistent with this understanding.

dx.doi.org/10.1021/jp401138h | J. Phys. Chem. B XXXX, XXX, XXX−XXX

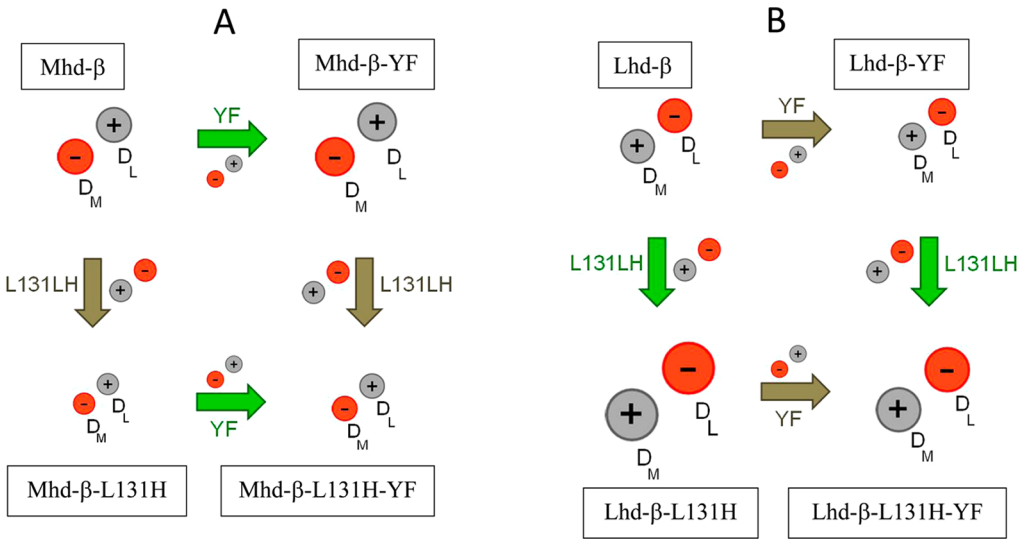

Figure 7. Schematic of the proposed localizations and relative magnitudes of electronic asymmetry of D* in the Lhd-β and Mhd-β mutants and for the L131LH and YF mutations. (A) The asymmetry inherent in the M-heterodimer is given in the upper left with a gray circle (positive charge) and red circle (negative charge) for the two macrocycles of D. The downward facing olive arrows indicate for L131LH a proposed effect that decreases electronic asymmetry of D*, while the right-facing green arrows indicate for YF a proposed smaller effect that increases electronic asymmetry of D*. The diameters of the pairs of circles indicate proposed relative magnitudes of electronic asymmetry. (B) Analogous diagram for the Lhd-β mutant set, where the effect of L131LH is to increase (green arrow) charge asymmetry of D*, and the effect of YF is to decrease (olive arrow) charge asymmetry of D*.

Further, these trends are mirrored in the photophysical properties of D* presented below. We consider first the ground state spectra of the Mhd mutant set, where the effects are somewhat more apparent than in the Lhd mutants. Comparing the NIR heterodimer absorption profiles of Mhd-β and Mhd-β-L131LH (Figure 3B), addition of L131LH results in a more well-defined absorption feature near 860 nm. A similar effect relates the spectra of Mhd-β-YF and Mhd-β-YF-L131LH. Net electron density in the M-heterodimer is inherently biased to $D_L^+D_M^-$; however, the hydrogen bond introduced to the ring V keto group of D_L by L131LH is expected to decrease this inherent electronic asymmetry, effectively adding oppositely biased $D_L^-D_M^+$ character. Thus the spectral comparisons of the effect of adding the hydrogen bond provided by L131LH to both Mhd-β and Mhd-β-YF are consistent with reduced electronic asymmetry of D* giving rise to a more P-like absorption band. Identical effects on the long-wavelength absorption band of D were reported previously for the Mhd and Mhd-L131LH mutants of *Rb. sphaeroides* and Stark effect measurements showed reduced charge asymmetry of D* in Mhd-L131LH compared to Mhd RCs.[60]

While the effects of changing the native Tyr M208 to a Phe and/or changing the native Phe L181 to a Tyr on ET to the L- and M-sides of the RC have been discussed extensively in terms of altering the free energies of $P^+B_L^-$ and $P^+B_M^-$, respectively, an effect on charge asymmetry in P* has not been reported previously to our knowledge. Analysis of the set of Mhd spectra suggests that the YF swap has an effect opposite to that induced by L131LH, i.e., YF increases the electronic asymmetry of D* in the M-heterodimer. This inference is drawn from the comparison of the Mhd-β and Mhd-β-YF ground state spectra and a similar comparison of the spectra of Mhd-β-L131LH and Mhd-β-L131LH-YF. Both pairings reveal a diminution of the long-wavelength absorbance of D in the presence of YF, opposite to the effect found for L131LH (Figure 3B). Inspection of the changes to the D absorption band among the four Mhd mutants suggests that the magnitude of the effect on the spectra by YF is smaller than that imparted by L131LH, which is chemically intuitive as well.

The above analysis of electronic asymmetry of D* in the Mhd mutant set is presented in pictorial form in Figure 7A. The red and gray circles indicate negative and positive charge, respectively, with D* in the Mhd-β mutant having inherent $D_L^+D_M^-$ electronic asymmetry. The green right-facing arrows depict a relatively small additive effect of the YF swap on charge asymmetry while the olive downward-facing arrows depict a relatively larger subtractive effect of L131LH on charge asymmetry in D*. The relative diameters of the gray/red circle pairs are intended as *qualitative* comparisons (larger versus smaller) of the magnitudes of electronic asymmetry.

The spectra in Figure 3A show reversed correlations among the four Lhd mutants, effects pictured in Figure 7B. More electron density on the L-moiety of D in the Lhd mutants is expected to increase the inherent $D_L^-D_M^+$ charge asymmetry of D*. The presence of L131LH should result in a broader, less-resolved long-wavelength absorbance of D. This effect is apparent (though small) in comparing the Lhd-β and Lhd-β-L131LH spectra, and is more clear from comparison of the Lhd-β-YF and Lhd-β-L131LH-YF spectra. The green downward-facing arrows in Figure 7B indicate that L131LH increases the charge asymmetry of D* in the L-heterodimer.

The effect of YF on the long-wavelength absorption band of the L-heterodimer is again reversed from the effect of L131LH, and reversed from the effect YF has on the M-heterodimer spectra. For example, comparing Lhd-β with Lhd-β-YF, the spectra indicate reduced charge asymmetry in the presence of YF (i.e., a more P-like absorption band). Overall, the spectral comparisons among the Lhd mutants in Figure 3A suggest that a larger effect is induced by L131LH than by YF. This mirrors the findings for the Mhd mutant set and is depicted in Figure 7B.

dx.doi.org/10.1021/jp401138h | *J. Phys. Chem. B* XXXX, XXX, XXX–XXX

Internal Conversion of D*. Increased CT character of D* in heterodimer RCs has long been associated with a much faster rate of internal conversion intrinsic to D* compared to P*. One explanation is that the fluctuations in the CT contribution in response to vibrations that alter the relative positions of the two macrocycles of the dimer may result in coupled electron−nuclear motion (Born−Oppenheimer breakdown) and increase nonradiative deactivation for D*.[41,68] For P* in wild-type RCs, the time constant for internal conversion is ∼100 ps in LDAO/Tris buffer and ∼200 ps in Deriphat/Tris buffer,[6−8,81,101−103] while for both the L-heterodimer and M-heterodimer these time constants are typically tens of picoseconds (Tables 1 and 2, column 6).[62,63] Following from the above discussions, we would expect that the increased electronic asymmetry conferred to the L-heterodimer upon addition of L131LH would give rise to faster D* internal conversion. Such results are observed (Table 1 column 6): Lhd-β-L131LH (16 ps) compared to Lhd-β (32 ps) and similarly Lhd-β-L131LH-YF (23 ps) compared to Lhd-β-YF (43 ps). Both comparisons indicate the time constant for D* internal conversion is about 2-fold smaller in the presence of L131LH. The effect of YF on D* internal conversion of the L-heterodimer is reversed and smaller, as evidenced by Lhd-β-YF (43 ps) compared to Lhd-β (32 ps) and similarly by Lhd-β-L131LH-YF (23 ps) compared to Lhd-β-L131LH (16 ps). These results give a factor of 1.3 to 1.4 larger time constant for D* internal conversion in the L-heterodimer in the presence of YF.

Parallel observations hold for the Mhd mutant set where the effects of the L131LH and YF mutations are again reversed from those found among the four Lhd mutants. Yet similar to the Lhd mutants, the magnitude of the effect of the YF swap on the time constant for D* internal conversion is smaller than the magnitude of effect of the L131LH mutation. Thus, the Mhd set reveals about a factor of 2 larger time constant linked to the presence of L131LH (reversed from the factor of 2 reduction for the Lhd mutants), but the factor of 2 change is essentially the same as found in the Lhd set. A previous study of two *Rb. sphaeroides* Mhd mutants (in LDAO) showed a similar larger time constant for D* internal conversion in Mhd-L131LH (80 ps) compared to Mhd (30 ps).[68] The magnitude of the effect of YF, though additive of CT character for the M-heterodimer, is again smaller than that of L131LH. In Figure 7, the qualitative indicators (gray/red circle diameters) of the relative magnitude of CT character of D* in the various mutants or associated with YF and L131LH were based on the above parallel effects on the long-wavelength ground state absorption of D and the time constants for D* internal conversion.

The smaller time constant of D* internal conversion in Mhd-β (28 ps) compared to Lhd-β (32 ps), suggests that D* electronic asymmetry might be slightly larger for the former than the latter. The same conclusion was reached previously from Stark effect measurements of the Mhd and Lhd mutants of *Rb. sphaeroides* (in LDAO/glycerol at 77K).[60] It seems clear, from both the long-wavelength ground state absorption band of D and the fast D* internal conversion time constant, that CT character of D* is largest in the Lhd-β-L131LH mutant and second largest in the Lhd-β-L131LH-YF mutant. Similarly it seems clear from the most P-like NIR absorption band of D and the largest D* internal conversion time constant, that D* electronic asymmetry is smallest in Mhd-β-L131LH, with Mhd-β-L131LH-YF ranking second smallest. These correlations are displayed in Figure 8 where the values of $(k_G)^{-1}$ (triangles) for all eight mutants are plotted left to right from smallest to largest. The resulting ordering of the mutants along the x-axis reveals the correlation between mutant and the degree of electronic asymmetry in D*. Specifically, in Figure 8, the mutants are found to be ranked from the largest amount of CT character of D* in Lhd-β-L131LH on the left to the smallest amount of CT character of D* in Mhd-β-L131LH on the right.

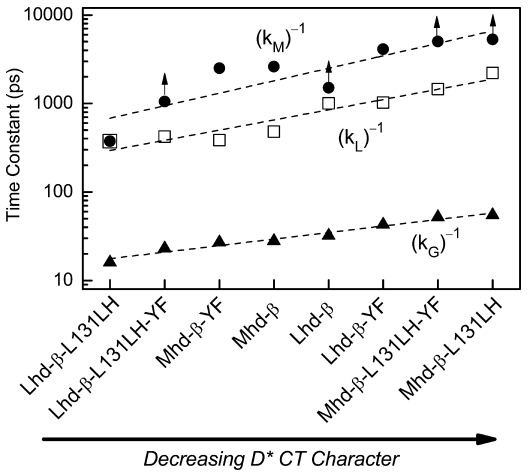

Figure 8. Plot of the time constants for the three D* decay processes, ET to β on the L-side $[(k_L)^{-1}]$, ET to H_M on the M-side $[(k_M)^{-1}]$, and internal conversion to the ground state $[(k_G)^{-1}]$, for the eight mutants demonstrating parallel correlations with the CT character of D*. The up-facing arrows indicate lower-limit values. The dashed lines are linear-fit trend lines.

Effect of Deriphat versus LDAO on Charge Asymmetry. For Lhd and Lhd-β, D* internal conversion is slightly faster in Deriphat than LDAO, while for Mhd and Mhd-β the opposite is found (Table 2, column 6). A simple interpretation of these results from an electronic asymmetry perspective is that D* in the L-heterodimer has more CT character in Deriphat than in LDAO, while for the M-heterodimer D* has more CT character in LDAO than Deriphat. Rephrasing this in terms of Figure 7, compared to LDAO, Deriphat may act on D* as does the hydrogen bond provided by L131LH, imparting $D_L^-D_M^+$ charge asymmetry to D*. In wild-type RCs in LDAO/glycerol/buffer at 77K, P* has net $P_L^+P_M^-$ character as determined by Stark effect measurements. It follows that addition of $P_L^-P_M^+$ character by Deriphat would reduce the electronic asymmetry of P* in wild-type RCs in Deriphat compared to LDAO. In other words, P* will have a more symmetric charge distribution in Deriphat. This might offer an explanation for why P* → ground state internal conversion in wild-type RCs is slower in Deriphat (∼200 ps) than in LDAO (∼100 ps).[6−8,81,101−103]

Electron Transfer in the Heterodimer Mutants. Our previous work compared branching of ET to the L- versus M-side in Lhd-β and Mhd-β in LDAO (see LDAO entries in Table 2). We found a larger value of the rate-constant ratio k_L/k_M for Mhd-β (3.7) compared to Lhd-β (1.5). This result is well-reproduced here in Deriphat where k_L/k_M is again larger for Mhd-β (>5) than for Lhd-β (1.5). These two results lead to the conclusion that the D* electron-density distribution in the M-heterodimer is superior to that of the L-heterodimer in supporting ET to the L-side of the RC and vice versa.[69]

We have expanded this understanding here with two sets of Lhd-β and Mhd-β mutants that incorporate L131LH and YF. As described above, we chose to use YF here to make the free energies of $D^+B_L^-$ and $D^+B_M^-$ more equal and thus better

dx.doi.org/10.1021/jp401138h | J. Phys. Chem. B XXXX, XXX, XXX−XXX

match the energetics of superexchange ET to the L- and M-sides (Figure 2D). Interestingly, we have found that YF also affects the charge asymmetry of D* but in a manner that is opposite to that of L131LH. For the Mhd mutants, because the direction of electronic asymmetry inherent to D* is strongly $D_L^+D_M^-$, we anticipated that the yields of ET to H_M would be even lower than in the Lhd mutants. This expectation was realized, with yields of ET to H_M <1% in all four Mhd mutants, from which lower-limit values of k_L/k_M may be determined. The time constants (inverse of the rate constants) and k_L/k_M ratios cited in the following are given in Table 1.

Point 1: If the conclusion from our earlier study on Lhd-β and Mhd-β is correct, that $D_L^-D_M^+$ CT character facilitates ET to H_M, the L131LH mutation should enhance ET to H_M because it pulls electron density toward the L-macrocycle. The relevant Lhd-β mutant pairings confirm this: k_L/k_M is smaller for Lhd-β-L131LH (1.0) than for Lhd-β (1.5) and smaller for Lhd-β-L131LH-YF (2.5) than for Lhd-β-YF (4.0). Though not a rigorous comparison, the lower-limit values of the Mhd set present similarly, e.g., a smaller lower-limit value for Mhd-β-L131LH (>2) compared to that for Mhd-β (>5).

Point 2: We have suggested above (from analysis of the ground state spectra and D* internal conversion time constants) that the YF swap imparts $D_L^+D_M^-$ CT character. This should enhance ET to the L-side at the expense of ET to the M-side. The comparisons that support such an effect of YF are that k_L/k_M is larger for Lhd-β-YF (4.0) than Lhd-β (1.5), and larger for Lhd-β-L131LH-YF (2.5) than Lhd-β-L131LH (1.0). Again, lower-limit values for the effects of YF on the Mhd mutants follow the predicted pattern (Table 1).

Point 3: The relative changes in the ET time constants among the mutants indicate that L131LH imparts effects of larger magnitude than does YF, as one might have expected. The same conclusion was also drawn above from analysis of the ground state spectra and time constants for internal conversion.

Point 4: Comparing the Lhd mutants, the rate constants k_G, k_L, and k_M are all larger (smaller time constants) in the presence of L131LH. For example, the three respective time constants for Lhd-β-L131LH (16 ps, 375 ps, 375 ps) are two- to four-fold smaller than for Lhd-β (32 ps, 1000 ps, 1500 ps). Similarly, YF has the effect of reducing all three rate constants (increasing the time constants) in the Lhd mutant set. These observations again hold but are reversed for the Mhd mutant set (qualified only by comparisons of lower-limit values for the k_M values).

Point 4 leads to the generalized observation that all three processes, internal conversion of D* and ET to both the L and M sides, are *uniformly faster* as a function of increased CT character of D*. The plots of the time constants for ET to the L-side (open squares), ET to the M-side (closed circles), and internal conversion (closed triangles) in Figure 8 clearly demonstrate the correlation between these observables and the extent of CT character of D*. The trends encompass all eight of the Lhd- and Mhd-containing mutants and time scales spanning over 2 orders of magnitude.

The plots in Figure 8 suggest that that a common fundamental physical factor or effect governs the essentially identical manner by which the degree of CT character of D* impacts all three D* decay rates (k_G, k_L, k_M). Faster internal conversion of P* in wild-type RCs than found for monomer BChl, and faster still for D* in heterodimer RCs, may derive from motions that modulate the spatial relationship of the two macrocycles of the dimer and thereby its electronic composition. This view invokes coupled electronic and nuclear motion (a breakdown of the Born−Oppenheimer approximation that underlies the Fermi Golden Rule). Recent work has suggested that L-side ET in wild-type and mutant RCs may be limited by protein dynamics.[104] For the heterodimers, protein motions could be the element that links CT character of D* with decay of D* via internal conversion and ET as displayed in Figure 8. Whether there exist protein motions that can simultaneously limit the rates of internal conversion and ET processes on time scales spanning over 2 orders of magnitude is not clear.

Other possibilities based on a more common Fermi Golden Rule perspective can be considered. It is difficult to see how the CT character of D* would give parallel impact among the eight mutants on the electronic-coupling factors (V^2) for the three different processes (ET to the L- and M-sides and D* internal conversion). A simpler link between the three D* decay processes may involve the impact of D* CT character on the respective Franck−Condon factors. Two possibilities are that increasing D* CT character may (1) make the D* potential energy surface more shallow (along some coordinates) and give move favorable overlap with the potential energy surfaces of the charge-separated products (for ET) and of the ground state (for internal conversion), and (2) increase the pigment−protein reorganization energy. The first point is simple and plausible. The second point involves a combination of factors. The two ET processes D* → $D^+\beta^-$ (L-side) and D* → $D^+H_M^-$ (M-side) likely lie in the Marcus activated or activationless regions. On the other hand, D* → ground state, like most internal conversion processes, would normally lie in the inverted region where the free energy change is much larger than the reorganization energy. However, this might not be the case for the heterodimers if the significant CT character of D* results in a sufficiently large reorganization energy. Whatever the combination of factors at play, the correlation in Figure 8 between D* charge asymmetry and the rate constants for the two ET processes and internal conversion is a noteworthy finding. This result along with the other spectral and kinetic data and comparisons obtained herein should entice in-depth theoretical investigation.

Transient Absorption Spectra of D* and D^+. The simplest picture of an excitonically coupled dimer of bacteriochlorins would predict weak mixing between the two monomeric Q_X absorption transitions compared to mixing of the Q_Y absorption transitions due to the smaller oscillator strengths of the former. This would lead to a zeroth-order model for the absorption spectrum of a BChl−BPh heterodimer having a Q_X band in the vicinity of 580−600 nm for the BChl moiety and one in the 530−550 nm region for the BPh moiety. It follows that one would expect the TA spectrum of D* and also of any charge-separated states formed that involve D^+ to display bleaching of both of these ground state bands. However, ESR and ENDOR measurements on heterodimer-containing RCs have shown that the hole (cation) in D^+ is localized essentially entirely on the BChl half of D.[39,105,106] Thus, following complete decay of D* (to either the ground state or charge-separated products), and under the assumption that the hole in D^+ is localized on the BChl moiety of D, one would expect to see only bleaching of the BChl-associated Q_X band in the TA spectrum. The ground state BPh-moiety absorption would be "recovered" upon localization of the hole on the BChl moiety, resulting in no net BPh bleaching in a TA difference spectrum (where the ground state spectrum is the subtracted reference).

dx.doi.org/10.1021/jp401138h | J. Phys. Chem. B XXXX, XXX, XXX−XXX

Such a result seems largely obtained for the Lhd-β-L131LH and Lhd-β-L131LH-YF mutants, for which no bleaching remains at ~550 nm at long time (Figure 6). Some bleaching at ~550 nm remains for Lhd-β and Lhd-β-YF at long time, which may indicate that the hole in D^+ is not entirely localized on the BChl moiety in these two mutants or that a more complex model for the ground state spectrum of D is needed. [Note that the 580−590 nm bleaching seen in the long time spectra in Figure 6 also has a contribution of bleaching of the ground state absorption of β due to its reduction (formation of $D^+\beta^-$), which would have to be taken into account in any further assessment of the oscillator strength of D absorption in this region.]

The fact that there is so little BChl Q_X bleaching in the D* spectra presents far more of a conundrum that has received little attention, though the first TA spectra of D* were reported over 20 years ago. The four Lhd D* spectra in Figure 5 exhibit virtually no 580−600 nm bleaching; the four Mhd D* spectra do show some bleaching at ~590 nm, but the ratio between the (putative) Q_X bleachings at ~550 nm and ~590 nm reconciles poorly with the nearly equal extinction coefficients and oscillator strengths of BPh and BChl Q_X absorptions in solution. If excitation were to be localized largely on one-half of a BChl−BPh heterodimer, one would expect that it would be on the BChl moiety because BChl* is lower in energy than BPh*. Either way, such a model would have a host of implications that are inconsistent with other observations. For example, one would expect to observe the excited state spectrum of BPh* or BChl*, which are well-known and do not exhibit the broad anion-like absorption features (600−700 nm) seen in Figure 5. Some combination of mixed molecular origin of the ~550 nm and ~590 absorption bands, differences in the relative extinction coefficients and widths of these bands compared to one another, new CT-like absorption features in the D* spectrum and band shifts on the Q_X absorption bands of the neighboring monomeric BChls seem to conspire to give little BChl bleaching in the observed D* spectra, with details still to be experimentally and theoretically resolved.

CONCLUSIONS

Analysis of the long-wavelength ground state absorption band of D, the rate of D*→ ground state (internal conversion), and the rate of ET from D* to the L-side versus to the M-side among a set of four L-heterodimer mutants and a parallel set of four M-heterodimer mutants reveals integral chromophore−protein and chromophore−chromophore interactions and photophysical properties that impact charge separation in the bacterial photosynthetic RC. The results presented here for the Lhd-β mutant compared to the Mhd-β mutant in Deriphat, and previously in LDAO, show that higher electron density on the M-macrocycle of D* favors ET to the L-side.[69] Prior theoretical studies on heterodimer[30] and wild-type RCs[13,14,16,18,25,29] indicate that the M-macrocycle of D or P has a stronger electronic interaction with B_L than B_M, and vice versa for the L-macrocycle of the dimer. Also, Stark effect measurements show that P* has a small net $P_L^+P_M^-$ CT character in wild-type RCs.[60] Together these three findings suggest that a design criterion to favor ET to the L-side would be to endow P* in the native RC with net $P_L^+P_M^-$ CT character.

The same ideas are supported here by our efforts to further match the energetics of ET on the two sides of the RC and alter the electronic factors for ET by manipulating the charge asymmetry in the excited primary donor. The addition of a hydrogen bond to the heterodimer via a His residue at L131 increases the inherent electron density on the L-macrocycle of D, thus increasing the electronic asymmetry of D* in the L-heterodimer and reducing it for D* in the M-heterodimer. Increased electronic asymmetry of D* translates into a broader, weaker D absorption in the NIR and, critically, faster internal conversion of D*. While building-in some nascent charge separation upon photon absorption may be useful, an attendant down side is that the inherent internal conversion lifetime of the excited primary electron donor (D* or P*) is shortened, placing greater pressure to shorten the time scale of moving an electron to the first acceptor.

We have shown here that the YF swap (placing Y at L181 and F at M208) acts electronically in a sense opposite to the L131LH mutation, increasing electronic asymmetry of D* for the M-heterodimer and decreasing it for the L-heterodimer. Consistent with this interpretation, the presence of YF—*the reverse of the native FY residue configuration*—is found to enhance ET to the L-side in the Lhd mutants. Extrapolating to the wild-type RC, the native residues FY (F at L181 and Y at M208) may thus have a disadvantageous shifting of electron density onto the L macrocycle of P, which, as shown here and previously, favors ET to the M side. Our results indicate that the magnitude of such native FY-induced electronic asymmetry in P* may not be large. Clearly Nature has chosen to utilize F at L181 and Y at M208 to help poise the free energy of $P^+B_L^-$ between that of P* and $P^+H_L^-$,[8,21,27] thus enabling the two-step mechanism of ET on the L-side and greatly favoring ET from P* to H_L via B_L over much slower ET via superexchange to H_M.

The Lhd-β-L131LH-YF mutant represents the best effort to date to equalize the free energies of the equivalent L- and M-side charge-separated states and equalize the mechanism of charge separation (superexchange on both sides). Electron transfer takes place to both L- and M-sides, on the hundreds of picoseconds time scale, which competes poorly with donor excited state (D*) internal conversion. Despite building in charge asymmetry that places significant electron density on the L-moiety of D* (enhancing ET to the M-side acceptors), ET to the L-side is still favored over the M-side in the Lhd-β-L131LH-YF mutant, but now only by a factor of about 2.5 compared to a factor of 30 for the wild-type RC. Our studies additionally reveal an unanticipated correlation of D* charge asymmetry and the rate constants for all three D* decay routes (ET to the L-side, ET to the M-side and internal conversion to the ground state) spanning the time scales of tens of picoseconds to several nanoseconds. Collectively, this work should provide rich grounds for comparisons to charge separation in Photosystem II, designing artificial charge-separation systems and fostering theoretical advances leading to even deeper appreciation of the primary energy-transformation processes of photosynthesis.

ASSOCIATED CONTENT

Supporting Information

Supporting Information includes the ground state absorption spectrum and P* TA spectrum for wild-type RCs and TA data analogous to that in Figure 4 for the other six mutants. This information is available free of charge via the Internet at http://pubs.acs.org.

AUTHOR INFORMATION

Corresponding Author

*E-mail: kirmaier@wustl.edu. Phone: 314-935-6480. Fax: 314-935-4481.

Notes

The authors declare no competing financial interest.

■ ACKNOWLEDGMENTS

C.K. and D.H. thank the National Science Foundation for supporting this work under Grant MCB-0948996. D.K.H., P.D.L., and C.L. acknowledge support by the United States Department of Energy under Contract No. DE-AC02-06CH11357 to the University of Chicago, LLC. C.L. was a participant in the Guest Faculty Research Program at Argonne National Laboratory and would like to thank Trinity Christian College for providing a one-semester sabbatical that allowed for his participation in this work.

■ REFERENCES

(1) Deisenhofer, J.; Epp, O.; Miki, K.; Huber, R.; Michel, H. Structure of the Protein Subunits in the Photosynthetic Reaction Center from *Rhodopseudomonas viridis* at 3 Å Resolution. *Nature* **1985**, *318*, 618−624.

(2) Allen, J. P.; Feher, G.; Yeates, T. O.; Komiya, H.; Rees, D. C. Structure of the Reaction Center from *Rhodobacter sphaeroides* R-26: The Cofactors. *Proc. Natl. Acad. Sci. U.S.A.* **1987**, *84*, 5730−5734.

(3) Chang, C.-H.; El-Kabbani, O.; Tiede, D. M.; Norris, J. R.; Schiffer, M. The Structure of the Membrane-Bound Photosynthetic Reaction Center from *Rhodobacter sphaeroides* R-26. *Proc. Natl. Acad. Sci. U.S.A.* **1991**, *30*, 5352−5360.

(4) Ermler, U.; Fritsch, G.; Buchanan, S. K.; Michel, H. Structure of the Photosynthetic Reaction Centre from *Rhodobacter sphaeroides* at 2.65 A Resolution: Cofactors and Protein−Cofactor Interactions. *Structure* **1994**, *2*, 925−936.

(5) Koepke, J.; Krammer, E. M.; Klingen, A. R.; Sebban, P.; Ullmann, G. M.; Fritzsch, G. pH Modulates the Quinone Position in the Photosynthetic Reaction Center from *Rhodobacter sphaeroides* in the Neutral and Charge Separated States. *J. Mol. Biol.* **2007**, *371*, 396−409.

(6) Heller, B. A.; Holten, D.; Kirmaier, C. Control of Electron Transfer to the L-Side versus the M-Side of the Photosynthetic Reaction Center. *Science* **1995**, *269*, 940−945.

(7) Kirmaier, C.; Weems, D.; Holten, D. M-Side Electron Transfer in Reaction Center Mutants with a Lysine near the Nonphotoactive B Bacteriochlorophyll. *Biochemistry* **1999**, *38*, 11516−11530.

(8) Kirmaier, C.; He, C.; Holten, D. Manipulating the Direction of Electron Transfer in the Bacterial Reaction Center by Swapping Phe for Tyr near $BChl_M$ (L181) and Tyr for Phe near $BChl_L$ (M208). *Biochemistry* **2001**, *40*, 12132−12139.

(9) Wakeham, M. C.; Jones, M. R. Rewiring Photosynthesis: Engineering Wrong-Way Electron Transfer in the Purple Bacterial Reaction Center. *Biochem. Soc. Trans.* **2005**, *133*, 851−857.

(10) Warshel, A. Role of the Chlorophyll Dimer in Bacterial Photosynthesis. *Proc. Natl. Acad. Sci. U.S.A.* **1980**, *77*, 3105−3109.

(11) Scherer, P. O. J.; Fischer, S. F. On the Stark-Effect for Bacterial Photosynthetic Reaction Centers. *Chem. Phys. Lett.* **1986**, *131*, 153−159.

(12) Parson, W. W.; Warshel, A. Spectroscopic Properties of Photosynthetic Reaction Centers. 2. Application of the Theory to *Rhodopseudomonas viridis*. *J. Am. Chem. Soc.* **1987**, *109*, 6152−6163.

(13) Plato, M.; Mobius, K.; Michel-Beyerle, M. E.; Bixon, M.; Jortner, J. Intermolecular Electronic Interactions in Bacterial Photosynthesis. *J. Am. Chem. Soc.* **1988**, *110*, 7279−7285.

(14) Warshel, A.; Creighton, S.; Parson, W. W. Electron-Transfer Pathways in the Primary Event of Bacterial Photosynthesis. *J. Phys. Chem.* **1988**, *92*, 2696−2701.

(15) Won, Y. D.; Friesner, R. A. On the Viability of the Superexchange Mechanism in the Primary Charge Separation Step of Bacterial Photosynthesis. *Biochim. Biophys. Acta* **1988**, *935*, 9−18.

(16) Michel-Beyerle, M. E.; Plato, M.; Deisenhofer, J.; Michel, H.; Bixon, M.; Jortner, J. Unidirectionality of Charge Separation in Reaction Centers of Photosynthetic Bacteria. *Biochim. Biophys. Acta* **1988**, *932*, 52−70.

(17) Friesner, R.; Won, Y. Spectroscopy and Electron Transfer Dynamics of the Bacterial Photosynthetic Reaction Center. *Biochim. Biophys. Acta* **1989**, *977*, 99−122.

(18) Scherer, P. O. J.; Fischer, S. F. Quantum Treatment of the Optical Spectra and the Initial Electron Transfer Process within the Reaction Center of *Rhodopseudomonas Viridis*. *Chem. Phys.* **1989**, *131*, 115−127.

(19) Bixon, M.; Jortner, J.; Michel-Beyerle, M. E.; Ogrodnik, A. A Superexchange Mechanism for the Primary Charge Separation in Photosynthetic Reaction Centers. *Biochim. Biophys. Acta* **1989**, *977*, 273−286.

(20) Warshel, A.; Aqvist, J. Electrostatic Correlation of Structure and Function in Proteins. *Chem. Scr.* **1989**, *29A*, 75−83.

(21) Parson, W. W.; Chu, Z. T.; Warshel, A. Electrostatic Control of Charge Separation in Bacterial Photosynthesis. *Biochim. Biophys. Acta* **1990**, *1017*, 251−272.

(22) Bixon, M.; Jortner, J.; Michel-Beyerle, M. E. On the Mechanism of Primary Charge Separation in Bacterial Photosynthesis. *Biochim. Biophys. Acta* **1991**, *1056*, 301−315.

(23) Thompson, M. A.; Zerner, M.; Fajer, J. A Theoretical-Examination of the Electronic-Structure and Excited-States of the Bacteriochlorophyll B Dimer from *Rhodopseudomonas viridis*. *J. Phys. Chem.* **1991**, *95*, 5693−5700.

(24) Thompson, M. A.; Zerner, M. A Theoretical Examination of the Electronic Structure and Spectroscopy of the Photosynthetic Reaction Center from *Rhodopseudomonas viridis*. *J. Am. Chem. Soc.* **1991**, *113*, 8210−8215.

(25) Lathrop, E. J. P.; Friesner, R. A. Simulation of Optical Spectra from the Reaction Center of *Rb. sphaeroides*. Effects of an Internal Charge-Separated State of the Special Pair. *J. Phys. Chem.* **1994**, 3056−3066.

(26) Reimers, J. R.; Hush, N. S. Nature of the Ground and First Excited-States of the Radical Cations of Photosynthetic Bacterial Reaction Centers. *Chem. Phys.* **1995**, *197*, 323−334.

(27) Gunner, M. R.; Nicholls, A.; Honig, B. Electrostatic Potentials in *Rhodopseudomonas viridis* Reaction Centers: Implications for the Driving Force and Directionality of Electron Transfer. *J. Phys. Chem.* **1996**, *100*, 4277−4291.

(28) Ivashin, N.; Kallebring, B.; Larsson, S.; Hansson, O. Charge Separation in Photosynthetic Reaction Centers. *J. Phys. Chem. B* **1998**, *102*, 5017−5022.

(29) Hasegawa, J.; Nakatsuji, H. Mechanism and Unidirectionality of Electron Transfer in the Photosynthetic reaction Center of *Rhodopseudomonas Viridis*: SAC-CI Theoretical Study. *J. Phys. Chem. B* **1998**, *102*, 10420−10430.

(30) Zhang, L. Y.; Friesner, R. A. Ab Initio Calculation of Electronic Coupling in the Photosynthetic Reaction Center. *Proc. Natl. Acad. Sci. U.S.A.* **1998**, *95*, 13603−13605.

(31) Kolbasov, D.; Scherz, A. Asymmetric Electron Transfer in Reaction Centers of Purple Bacteria Strongly Depends on Different Electron Matrix Elements in the Active and Inactive Branches. *J. Phys. Chem. B* **2000**, *104*, 1802−1809.

(32) Pudlak, M.; Pincak, R. The Role of Accessory Bacteriochlorophyll in the Primary Charge Transfer in the Photosynthetic Reaction Center. *Chem. Phys. Lett.* **2001**, *342*, 587−592.

(33) Pudlak, M.; Pincak, R. Modeling Charge Transfer in the Photosynthetic Reaction Center. *Phys. Rev. E* **2003**, *68*, 069011−069017.

(34) LeBard, D. N.; Kapko, V.; Matyushov, D. V. Energetics and Kinetics of Primary Charge Separation in Bacterial Photosynthesis. *J. Phys. Chem. B* **2008**, *112*, 10322−10342.

(35) Pudlak, M.; Pincak, R. Electronic Pathway in Reaction Centers from *Rhodobacter sphaeroides* and *Chloroflexus aurantiacus*. *J. Biol. Phys.* **2010**, *36*, 273−289.

(36) Eisenmayer, T. J.; de Groot, H. J. M.; van de Wetering, E.; Neugebauer, J.; Buda, F. Mechanism and Reaction Coordinate of

Directional Charge Separation in Bacterial Reaction Centers. *J. Phys. Chem. Lett.* **2012**, *3*, 694−697.
(37) Lendzian, F.; Huber, M.; Issacson, R. A.; Endeward, B.; Plato, M.; Bonigk, B.; Mobius, K.; Lubitz, W.; Feher, G. The Electronic-Structure of the Primary Donor Cation-Radical in *Rhodobacter sphaeroides* R-26 - Endor and Triple-Resonance Studies in Single-Crystals of Reaction Centers. *Biochim. Biophys. Acta* **1993**, *1183*, 139−160.
(38) Rautter, J.; Lendzian, F.; Lubitz, W.; Wang, S.; Allen, J. P. Comparative Study of Reaction Centers from Photosynthetic Purple Bacteria: Electron Paramagnetic Resonance and Electron Nuclear Double Resonance Spectroscopy. *Biochemistry* **1994**, *33*, 12077−12084.
(39) Rautter, J.; Lendzian, F.; Schulz, C.; Fetsch, A.; Kuhn, M.; Lin, X.; Williams, J. C.; Allen, J. P.; Lubitz, W. Endor Studies of the Primary Donor Cation-Radical in Mutant Reaction Centers of *Rhodobacter sphaeroides* with Altered Hydrogen-Bond Interactions. *Biochemistry* **1995**, *34*, 8130−8143.
(40) Artz, K.; Williams, J. C.; Allen, J. P.; Lendzian, F.; Rautter, J.; Lubitz, W. Relationship between the Oxidation Potential and Electron Spin Density of the Primary Electron Donor in Reaction Centers from *Rhodobacter sphaeroides*. *Proc. Natl. Acad. Sci. U.S.A.* **1997**, *94*, 13582−13587.
(41) McDowell, L. M.; Kirmaier, C.; Holten, D. Charge Transfer and Charge Resonance States of the Primary Electron Donor in Wild-Type and Mutant Bacterial Reaction Centers. *Biochim. Biophys. Acta* **1990**, *1020*, 239−246.
(42) Steffen, M. A.; Lao, K.; Boxer, S. G. Dielectric Asymmetry in the Photosynthetic Reaction Center. *Science* **1994**, *264*, 810−816.
(43) Meech, S. R.; Hoff, A. J.; Wiersma, D. A. Role of Charge-Transfer States in Bacterial Photosynthesis. *Proc. Natl. Acad. Sci. U.S.A.* **1986**, *83*, 9464−9468.
(44) Boxer, S. G.; Middendorf, T. R.; Lockhart, D. J. Reversible Photochemical Holeburning in *Rhodopseudomonas viridis* Reaction Centers. *FEBS Lett.* **1986**, *200*, 237−241.
(45) Tang, D.; Jankowiak, R.; Small, G. J.; Tiede, D. M. Structured Hole Burned Spectra of the Primary Donor State Absorption Region of *Rhodopseudomonas viridis*. *Chem. Phys.* **1989**, *131*, 99−113.
(46) Won, Y. D.; Friesner, R. A. Theoretical Studies of Photochemical Hole Burning in Photosynthetic Bacterial Reaction Centers. *J. Phys. Chem.* **1988**, *92*, 2214−2219.
(47) Lockhart, D. J.; Boxer, S. G. Stark-Effect Spectroscopy of *Rhodobacter sphaeroides* and *Rhodopseudomonas viridis* Reaction Centers. *Proc. Natl. Acad. Sci. U.S.A.* **1988**, *85*, 107−111.
(48) Losche, M.; Feher, G.; Okamura, M. Y. The Stark-Effect in Reaction Centers from *Rhodobacter sphaeroides* R-26 and *Rhodopseudomonas viridis*. *Proc. Natl. Acad. Sci. U.S.A.* **1987**, *84*, 7537−7541.
(49) Hammes, S. L.; Mazzola, L.; Boxer, S. G.; Gaul, D. F.; Schenck, C. C. Stark Spectroscopy of the *Rhodobacter sphaeroides* Reaction Center Heterodimer Mutant. *Proc. Natl. Acad. Sci. U.S.A.* **1990**, *87*, 5682−5686.
(50) Zhou, H.; Boxer, S. G. Charge Resonance Effects on Electronic Absorption Line Shapes: Application to the Heterodimer Absorption of Bacterial Photosynthetic Reaction Centers. *J. Phys. Chem. B* **1997**, *101*, 5759−5766.
(51) Zhou, H.; Boxer, S. G. Probing Excited-State Electron Transfer by Resonance Stark Spectroscopy. 1. Experimental Results for Photosynthetic Reaction Centers. *J. Phys. Chem. B* **1998**, *102*, 9139−9147.
(52) Zhou, H.; Boxer, S. G. Probing Excited-State Electron Transfer by Resonance Stark Spectroscopy. 2. Theory and Application. *J. Phys. Chem. B* **1998**, *102*, 9148−9160.
(53) van Dijk, B.; Hoff, A. J.; Shkuropatov, A. Y. Electrooptical Properties of Different Redox States of Native and Modified Reaction Centers of *Rhodobacter sphaeroides*. *J. Phys. Chem. B* **1998**, *102*, 8091−8099.
(54) DiMagno, T. J.; Bylina, E. J.; Angerhofer, A.; Youvan, D. C.; Norris, J. R. Stark-Effect in Wild-Type and Heterodimer-Containing Reaction Centers from *Rhodobacter capsulatus*. *Biochemistry* **1990**, *29*, 899−907.
(55) Thurnauer, M.; Katz, J. J.; Norris, J. R. Triplet-State in Bacterial Photosynthesis - Possible Mechanisms of Primary Photo-Act. *Proc. Natl. Acad. Sci. U.S.A.* **1975**, *72*, 3270−3274.
(56) Takiff, L.; Boxer, S. G. Phosphorescence from the Primary Electron-Donor in *Rhodobacter sphaeroides* and *Rhodopseudomonas viridis* Reaction Centers. *Biochim. Biophys. Acta* **1988**, *932*, 325−334.
(57) Dijkman, J. A.; den Blanken, H. J.; Hoff, A. J. Towards a New Taxonomy of Photosynthetic Bacteria: ADMR-Monitored Triplet Difference Spectroscopy of Reaction Center Pigment−Protein Complexes. *Isr. J. Chem.* **1989**, *28*, 141−148.
(58) Norris, J. R.; Budil, D. E.; Gast, P.; Chang, C.-H.; El-Kabbani, O.; Schiffer, M. Correlation of Paramagnetic States and Molecular Structure in Bacterial Photosynthetic Reaction Centers: The Symmetry of the Primary Electron Donor in *Rhodopseudomonas viridis* and *Rhodobacter sphaeroides* R-26. *Proc. Natl. Acad. Sci. U.S.A.* **1989**, *86*, 4335−4339.
(59) Boxer, S. G.; Goldstein, R. A.; Lockhart, D. J.; Middendorf, T. R.; Takiff, L. Excited-States, Electron-Transfer Reactions, and Intermediates in Bacterial Photosynthetic Reaction Centers. *J. Phys. Chem.* **1989**, *93*, 8280−8294.
(60) Moore, L. J.; Zhou, H.; Boxer, S. G. Excited-State Electronic Asymmetry of the Special Pair in Photosynthetic Reaction Center Mutants: Absorption and Stark Spectroscopy. *Biochemistry* **1999**, *38*, 11949−11960.
(61) Bylina, E. J.; Youvan, D. C. Directed Mutations Affecting Spectroscopic and Electron-Transfer Properties of the Primary Donor in the Photosynthetic Reaction Center. *Proc. Natl. Acad. Sci. U.S.A.* **1988**, *85*, 7226−7230.
(62) Kirmaier, C.; Holten, D.; Bylina, E. J.; Youvan, D. C. Electron Transfer in a Genetically Modified Bacterial Reaction Center Containing a Heterodimer. *Proc. Natl. Acad. Sci. U.S.A.* **1988**, *85*, 7562−7566.
(63) McDowell, L. M.; Gaul, D.; Kirmaier, C.; Holten, D.; Schenck, C. C. Investigation into the Source of Electron Transfer Asymmetery in Bacterial Reaction Centers. *Biochemistry* **1991**, *30*, 8315−8322.
(64) Camara-Artigas, A.; Magee, C.; Goetsch, A.; Allen, J. P. The Structure of the Heterodimer Reaction Center from *Rhodobacter sphaeroides* at 2.55 A Resolution. *Photosynth. Res.* **2002**, *74*, 87−93.
(65) Chirino, A. J.; Lous, E. J.; Huber, M.; Allen, J. P.; Schenck, C. C.; Paddock, M. L.; Feher, G.; Rees, D. C. Crystallographic Analysis of Site-Directed Mutants of the Photosynthetic Reaction Center from *Rhodobacter sphaeroides*. *Biochemistry* **1994**, *33*, 4584−4593.
(66) Ponomarenko, N. S.; Li, L.; Marino, A. R.; Tereshko, V.; Ostafin, A.; Popova, J. A.; Bylina, E. J.; Ismagilov, R. F.; Norris, J. R. Structural and Spectropotentiometric Analysis of *Blastochloris viridis* Heterodimer Mutant Reaction Center. *Biochim. Biophys. Acta, Biomembr* **2009**, *1788*, 1822−1831.
(67) Kirmaier, C.; Bylina, E. J.; Youvan, D. C.; Holten, D. Subpicosecond Formation of the Intradimer Charge-Transfer State [$BChl_{LP}^{+}BPh_{MP}^{-}$] in Reaction Centers from the His(M200)Leu Mutant of *Rhodobacter capsulatus*. *Chem. Phys. Lett.* **1989**, *159*, 251−257.
(68) Laporte, L. L.; Palaniappan, V.; Davis, D. G.; Kirmaier, C.; Schenck, C. C.; Holten, D.; Bocian, D. F. Influence of Electronic Asymmetry on the Spectroscopic and Photodynamic Properties of the Primary Electron Donor in the Photosynthetic Reaction Center. *J. Phys. Chem.* **1996**, *100*, 17696−17707.
(69) Kirmaier, C.; Bautista, J. A.; Laible, P. D.; Hanson, D. K.; Holten, D. Probing the Contribution of Electronic Coupling to the Directionality of Electron Transfer in Photosynthetic Reaction Centers. *J. Phys. Chem. B* **2005**, *109*, 24160−24172.
(70) Khatypov, R. A.; Khmelnitskiy, A. Y.; Khristin, A. M.; Fufina, T. Y.; Vasilieva, L. G.; Shuvalov, V. A. Primary Charge Separation within P870* in Wild Type and Heterodimer Mutants in Femtosecond Time Domain. *Biochim. Biophys. Acta* **2012**, *1817*, 1392−1398.
(71) Allen, J. P.; Artz, K.; Lin, X.; Williams, J. C.; Ivancich, A.; Albouy, D.; Mattioli, T. A.; Fetsch, A.; Kuhn, M.; Lubitz, W. Effects of

Hydrogen Bonding to a Bacteriochlorophyll−Bacteriopheophytin Dimer in Reaction Centers of *Rhodobacter sphaeroides*. *Biochemistry* **1996**, *35*, 6612−6619.
(72) Davis, D.; Dong, A.; Caughey, W. S.; Schenck, C. C. Energetics of the Oxidized Primary Donor in Wt and Hetero-Dimer Mutant Reaction Centers. *FASEB J.* **1992**, *61*, A153−A153.
(73) Kirmaier, C.; Gaul, D.; DeBey, R.; Holten, D.; Schenck, C. C. Charge Separation in a Reaction Center Incorporating Bacteriochlorophyll in Place of Photoactive Bacteriopheophytin. *Science* **1991**, *251*, 922−927.
(74) Heller, B. A.; Holten, D.; Kirmaier, C. Characterization of Bacterial Reaction Centers Having Mutations of Aromatic Residues in the Binding Site of the Bacteriopheophytin Intermediary Electron Carrier. *Biochemistry* **1995**, *34*, 5294−5302.
(75) Fajer, J.; Borg, D. C.; Forman, A.; Dolphin, D.; Felton, R. H. Anion Radical of Bacteriochlorophyll. *J. Am. Chem. Soc.* **1973**, *95*, 2739−2741.
(76) Fajer, J.; Brune, D. C.; Davis, M. S.; Forman, A.; Spaulding, L. D. Primary Charge Separation in Bacterial Photosynthesis: Oxidized Chlorophylls and Reduced Pheophytin. *Proc. Natl. Acad. Sci. U.S.A.* **1975**, *72*, 4956−4960.
(77) Alden, R. G.; Parson, W. W.; Chu, Z. T.; Warshel, A. Orientation of the OH Dipole of Tyrosine (M)210 and Its Effect on Electrostatic Energies in Photosynthetic Bacterial Reaction Centers. *J. Phys. Chem.* **1996**, *100*, 16761−16770.
(78) Kirmaier, C.; Laible, P. D.; Hanson, D. K.; Holten, D. B-Side Electron Transfer to Form $P^+H_B^-$ in Reaction Centers from the F(L181)Y/Y(M208)F Mutant of *Rhodobacter capsulatus*. *J. Phys. Chem. B* **2004**, *108*, 11827−11832.
(79) Kirmaier, C.; Laible, P. D.; Hanson, D. K.; Holten, D. B-side Charge Separation in Bacterial Photosynthetic Reaction Centers: Nanosecond-Timescale Electron Transfer from H_B^- to Q_B. *Biochemistry* **2003**, *42*, 2016−2024.
(80) Laible, P. D.; Kirmaier, C.; Udawatte, C. S. M.; Hofman, S. J.; Holten, D.; Hanson, D. K. Quinone Reduction via Secondary B-Branch Electron Transfer in Mutant Bacterial Reaction Centers. *Biochemistry* **2003**, *42*, 1718−1730.
(81) Chuang, J. I.; Boxer, S. G.; Holten, D.; Kirmaier, C. High Yield of M-Side Electron Transfer in Mutants of *Rhodobacter capsulatus* Reaction Centers Lacking the L-Side Bacteriopheophytin. *Biochemistry* **2006**, *45*, 3845−3851.
(82) Carter, B.; Boxer, S. G.; Holten, D.; Kirmaier, C. Trapping the $P^+B_L^-$ Initial Intermediate State of Charge Separation in Photosynthetic Reaction Centers from *Rhodobacter capsulatus*. *Biochemistry* **2009**, *48*, 2571−2573.
(83) Carter, B.; Boxer, S. G.; Holten, D.; Kirmaier, C. Photochemistry of a Bacterial Photosynthetic Reaction Center Missing the Initial Bacteriochlorophyll Electron Acceptor. *J. Phys. Chem. B* **2012**, *116*, 9971−9982.
(84) Jia, Y.; DiMagno, T. J.; Chan, C.-K.; Wang, Z.; Du, M.; Hanson, D. K.; Schiffer, M.; Norris, J. R.; Fleming, G. R.; Popov, M. S. Primary Charge Separation in Mutant Reaction Centers of *Rhodobacter capsulatus*. *J. Phys. Chem.* **1993**, *97*, 13180−13191.
(85) Nagarajan, V.; Parson, W. W.; Davis, D.; Schenck, C. C. Kinetics and Free Energy Gaps of Electron Transfer Reactions in *Rhodobacter sphaeroides* Reaction Centers. *Biochemistry* **1993**, *32*, 12324−12336.
(86) Hamm, P.; Gray, K. A.; Oesterhelt, D.; Feick, R.; Scheer, H.; Zinth, W. Subpicosecond Emission Studies of Bacterial Reaction Centers. *Biochim. Biophys. Acta* **1993**, *1142*, 99−105.
(87) Beekman, L. M. P.; van Stokkum, I. H. M.; Monshouwer, R.; Rijnders, A. J.; McGlynn, P.; Visschers, R. W.; Jones, M. R.; van Grondelle, R. Primary Electron Transfer in Membrane-Bound Reaction Centers with Mutations at the M210 Position. *J. Phys. Chem.* **1996**, *100*, 7256−7268.
(88) Streltsov, A. M.; Vulto, S. I. E.; Shkuropatov, A. Y.; Hoff, A. J.; Aartsma, T. J.; Shuvalov, V. A. B_A and B_B Absorbance Perturbations Induced by Coherent Nuclear Motions in Reaction Centers from Rhodobacter sphaeroides upon 30-fs Excitation of the Primary Donor. *J. Phys. Chem. B* **1998**, *102*, 7293−7298.
(89) Allen, J. P.; Williams, J. C. Relationship Between the Oxidation Potential of the Bacteriochlorophyll Dimer and Electron Transfer in Photosynthetic Reaction Centers. *J. Bioenerg. Biomembr.* **1995**, *27*, 275−283.
(90) Williams, J. C.; Alden, R. G.; Murchison, H. A.; Peloquin, J. M.; Woodbury, N. W.; Allen, J. P. Effects of Mutations near the Bacteriochlorophylls in Reaction Centers from *Rhodobacter sphaeroides*. *Biochemistry* **1992**, *31*, 11029−11037.
(91) Nabedryk, E.; Breton, J.; Williams, J. C.; Allen, J. P.; Kuhn, M.; Lubitz, W. FTIR Characterization of the Primary Electron Donor in Double Mutants Combining the Heterodimer HL(M202) with the LH(L131), HF(L168), FH(M197), or LH(M160) Mutations. *Spectrochim. Acta, Part A* **1998**, *54*, 1219−1230.
(92) Muh, F.; Lendzian, F.; Roy, M.; Williams, J. C.; Allen, J. P.; Lubitz, W. Pigment−Protein Interactions in Bacterial Reaction Centers and Their Influence on Oxidation Potential and Spin Density Distribution of the Primary Donor. *J. Phys. Chem. B* **2002**, *106*, 3226−3236.
(93) Tang, C.-K.; Williams, J. C.; Taguchi, A. K. W.; Allen, J. P.; Woodbury, N. W. $P^+H_A^-$ Charge Recombiantion Rate Constant in *Rhodobacter sphaeroides* Reaction Centers is Independent of P/P^+ Midpoint Potential. *Biochemistry* **1999**, *38*, 8794−8799.
(94) Nabedryk, E.; Allen, J. P.; Taguchi, A. K. W.; Williams, J. C.; Woodbury, N. W.; Breton, J. Fourier-Transform Infrared Study of the Primary Electron-Donor in Chromatophores of *Rhodobacter sphaeroides* with Reaction Centers Genetically Modified at Residue-M160 and Residue-L131. *Biochemistry* **1993**, *32*, 13879−13885.
(95) Mattioli, T. A.; Williams, J. C.; Allen, J. P.; Robert, B. Changes in Primary Donor Hydrogen-Bonding Interactions in Mutant Reaction Centers from *Rhodobacter sphaeroides* - Identification of the Vibrational Frequencies of All the Conjugated Carbonyl Groups. *Biochemistry* **1994**, *33*, 1636−1643.
(96) Lin, X.; Murchison, H. A.; Nagarajan, V.; Parson, W. W.; Allen, J. P.; Williams, J. C. Specific Alteration of the Oxidation Potential of the Electron Donor in Reaction Centers from *Rhodobacter sphaeroides*. *Proc. Natl. Acad. Sci. U.S.A.* **1994**, *91*, 10265−10269.
(97) Faries, K. M.; Kressel, L. L.; Wander, M. J.; Holten, D.; Laible, P. D.; Kirmaier, C.; Hanson, D. K. High Throughput Engineering to Revitalize a Vestigial Electron Transfer Pathway in Bacterial Photosynthetic Reaction Centers. *J. Biol. Chem.* **2012**, *287*, 8507−8514.
(98) Laible, P. D.; Scott, H. N.; Henry, L.; Hanson, D. K. Towards Higher-Throughput Membrane Protein Production for Structure Genomics Initiatives. *J. Struct. Funct. Genomics* **2004**, *5*, 167−173.
(99) Bylina, E. J.; Kirmaier, C.; McDowell, L. M.; Holten, D.; Youvan, D. C. Influence of an Amino Acid Residue on the Optical Properties and Electron Transfer Dynamics of a Photosynthetic Reaction Center Complex. *Nature* **1988**, *336*, 182−184.
(100) Kirmaier, C.; Cua, A.; He, C.; Holten, D.; Bocian, D. F. Probing M-Branch Electron Transfer and Cofactor Environment in the Bacterial Photosynthetic Reaction Center by the Addition of a Hydrogen Bond to the M-side Bacteriopheophytin. *J. Phys. Chem. B* **2002**, *106*, 495−503.
(101) Breton, J.; Martin, J. L.; Lambry, J. C.; Robles, S. J.; Youvan, D. C. Ground State and Femtosecond Transient Absorption Spectroscopy of a Mutant of *Rhodobacter capsulatus* which Lacks the Initial Electron Acceptor Bacteriopheophyrin. In *Structure and Function of Bacterial Photosynthetic Reaction Centers*; Michel-Beyerle, M. E., Ed.; Springer-Verlag: New York, 1990; pp 293−302.
(102) Chuang, J. I.; Boxer, S. G.; Holten, D.; Kirmaier, C. Temperature Dependence of Electron Transfer to the M-Side Bacteriopheophytin in *Rhodobacter capsulatus* Reaction Centers. *J. Phys. Chem. B* **2008**, *112*, 5487−5499.
(103) Kirmaier, C.; Laible, P. D.; Hinden, E.; Hanson, D. K.; Holten, D. Detergent Effects on Primary Charge Separation in Wild-Type and Mutant *Rhodobacter capsulatus* Reaction Centers. *Chem. Phys.* **2003**, *294*, 305−318.
(104) Wang, H. Y.; Lin, S.; Allen, J. P.; Williams, J. C.; Blankert, S.; Laser, C.; Woodbury, N. W. Protein Dynamics Control the Kinetics of

Initial Electron Transfer in Photosynthesis. *Science* **2007**, *316*, 747−750.

(105) Huber, M.; Isaacson, R. A.; Abresch, E. C.; Gaul, D.; Schenck, C. C.; Feher, G. Electronic Structure of the Oxidized Primary Electron Donor of the HL(M202) and HL(L173) Heterodimer Mutants of the Photosynthetic Bacterium *Rhodobacter sphaeroides*: ENDOR on Single Crystals of Reaction Centers. *Biochim. Biophys. Acta* **1996**, *1273*, 108−128.

(106) Ponomarenko, N. S.; Poluektov, O. G.; Bylina, E. J.; Norris, J. R. Electronic Structure of the Primary Electron Donor of *Blastochloris viridis* Heterodimer Mutants: High-Field ESR Study. *Biochim. Biophys. Acta* **2010**, *1797*, 1617−1626.